



# Use of major ions to evaluate groundwater chemistry and identify hydrochemical processes in a shallow coastal aquifer in southeast Brazil

Carlos Alberto de Carvalho Filho<sup>1</sup> · Virgílio Lopardi Bomtempo<sup>1</sup> · Stela Dalva Santos Cota<sup>1</sup> · Paulo Sérgio Pelógia Minardi<sup>1</sup> · Ricardo Gomes Passos<sup>1</sup>

Received: 27 September 2021 / Accepted: 25 June 2022 / Published online: 23 August 2022  
© The Author(s), under exclusive licence to Springer-Verlag GmbH Germany, part of Springer Nature 2022

## Abstract

Coastal aquifers of southeastern Brazil have a fundamental role in economic and social terms, as it is a densely populated region with intense economic activity. The present research was carried out in the coastal region of the State of Rio de Janeiro and enclosed the Brazilian Nuclear Power Plants (NPP) site. The study aimed to assess the hydrochemistry of the shallow aquifer at the NPP's site and surroundings. The hydrochemical study was carried out based on data from 12 water samples, collected in October 2018, in which parameters were measured in situ (such as electrical conductivity, total dissolved solids, temperature, and pH) and in the laboratory (such as alkalinity;  $\text{Ca}^{2+}$ ,  $\text{Mg}^{2+}$ ,  $\text{Na}^+$ ,  $\text{K}^+$ ;  $\text{Cl}^-$ ,  $\text{SO}_4^{2-}$ , and silicon). Using Piper and Chadha diagrams, the research identified four water types: Group 1 ( $\text{Ca}^{2+}\text{-Na}^+\text{-HCO}_3^-$ ), Group 2 ( $\text{Ca}^{2+}\text{-HCO}_3^-$ ), Group 3 [ $\text{Ca}^{2+}$  ( $\text{Na}^+$  rich) $\text{-HCO}_3^-$ ], and Group 4 ( $\text{Na}^+\text{-Cl}^-$ ). From the hillsides towards the beach line, the research results suggest a hydrochemical evolution of local groundwater from Group 1 (high rainwater influence), passing through Group 3 (intermediate between Group 1 and 2) and Group 2 (rock influence), to Group 4 (seawater like). The waters of groups 1 to 3 showed potential for base cation exchange (softening or freshening process), while, in Group 4, the potential is for reverse cation exchange (hardening or salinizing process). In a general hydrogeology context, the methods and applied techniques proved to be particularly efficient in identifying potential hydrochemical processes. Noteworthy is the freshening cation exchange identified in the shallow aquifer at NPP's site. Therefore, theoretically, in case of an accidental release of radionuclides from the NPP to the aqueous phase, the local clay lenses can capture the divalent cation  $\text{Ra}^{2+}$  in a natural contamination attenuation process.

**Keywords** Hydrochemistry · Coastal aquifer · Hydrochemical processes · Seawater interference

## Introduction

All industrial activity can affect the environment, with water resources being one of the most vulnerable environmental compartments for human actions. In this context, the International Atomic Energy Agency (IAEA) conducted a Coordinated Research Project (CRP) with the objective of better evaluating the hydrogeological conditions in the geological configuration of Nuclear Power Plants (NPP's) sites using specific isotope techniques coupled with classic hydrochemical ones (IAEA 2021). The results of the CRP aimed at providing basic information that could be used for predicting chemical behavior and the fate of radioactive and conventional contaminants that may be released into groundwater during normal operations conditions or due to an accident.

✉ Carlos Alberto de Carvalho Filho  
cacf@cdtn.br

Virgílio Lopardi Bomtempo  
vlb@cdtn.br

Stela Dalva Santos Cota  
sdsc@cdtn.br

Paulo Sérgio Pelógia Minardi  
pspm@cdtn.br

Ricardo Gomes Passos  
ricardo.passos@cdtn.br

<sup>1</sup> Nuclear Technology Development Center (CDTN/ CNEN), Av. Presidente Antônio Carlos 6627, Pampulha, Belo Horizonte, Minas Gerais 31270-901, Brazil

A detailed understanding of groundwater hydrochemistry is relevant for the protection of the water resources as a whole to establish reference values for water quality and quantity for sustainable groundwater management (Sefie et al. 2018; Tizro and Voudouris 2008), mainly in regions where water is demanded by different uses with risk of conflicts. Previous works in the literature report the importance of knowing the hydrochemistry of water, especially for safe drinking and agriculture (Mechal et al. 2022; Sarkar et al. 2022).

The Brazilian nuclear power plant complex known as “Centrais Nucleares Almirante Álvaro Alberto-CNAAA” comprises two nuclear power plants in full operation, Angra I and Angra II, and another under construction (Angra III). The complex is situated in the municipality of Angra dos Reis (RJ), southeastern Brazilian coastline, near the limits of the states of São Paulo (SP) and Rio de Janeiro (RJ), the first and third largest Brazilian states in population, respectively.

Coastal aquifers of southeastern Brazil have a fundamental role in economic and social terms, as it is a densely populated region with intense economic activity. These aquifers belong to the Atlantic Coastal Hydrogeological Province (Bocanegra et al. 2010), extending intermittently along the Atlantic coast, from Uruguay (in the south) to the north, passing through Brazil, Guianas, Venezuela, and Colombia. Coastal aquifers systems such as these are very vulnerable to salinity caused by the influence of seawater, which is one of the significant threats to groundwater quality (Khan et al. 2021). In addition, according to Zhang and Zhang (2021), a better understanding of submarine groundwater discharge and coastal groundwater is urgent and important to clarify global environmental changes. However, even in coastal systems, the saline intrusion phenomenon occurs along with several other possible hydrodynamic processes, therefore not being the only one to dictate the quality of the water. Other factors that threaten groundwater quality can be related to land use and occupation and human activities, such as the presence of industries, domestic effluents, and agriculture (Xiao et al. 2021), as well as both natural and anthropogenic factors (Bodrud-Doza et al. 2019). On the other hand, hydrogeological features may be responsible for improving water quality. In some hydrogeological contexts, cation exchange may be the main natural factor controlling groundwater chemistry (Okofu et al. 2021). In the study area, clay lenses (a local geological feature) may be beneficial for ion exchange and pollutants capture.

The objective of this study was to assess the hydrochemistry of a shallow aquifer at the location of Brazilian nuclear power plants and the surrounding area. Classical hydrochemical diagrams, scatter graphics, and hydrochemical indexes were used to identify the types and sources of water, the water mixtures, and the potentially feasible hydrochemical processes related to seawater influence, such as ion exchange

and salinization. This work aimed to contribute to the knowledge of the study location situation as a diagnosis of water quality and its dynamic in a region that has the potential to suffer radiological impacts due to the presence of the NPPs. The presence of clay lenses in the region is also a situation that was hypothesized to be beneficial for ion exchange and detention of radioactive metals in case of accidents; aspects few explored in previous similar works. Specifically, identifying the potential for cation exchange reactions is essential where nuclear or radioactive facilities are involved. It is not new that radium, being a divalent cation, similar to calcium and magnesium, can also be removed from water by the cation exchange process (EPA 1983; Nirdosh 1984; Bi et al. 2016; Robin et al. 2017). Thus, natural cation exchange can attenuate aquifer contamination by radium. In addition to the local diagnosis and hydrological dynamic assessment, which has large importance for the local economy and population health, the study is about a hydrogeologic scenario that can be easily found in other parts of the world.

## Site description

The study was carried out in a highly touristic coastal region of the State of Rio de Janeiro (Fig. 1), about 20 km from the city of Angra dos Reis (204 thousand inhabitants), 120 km from the city of Rio de Janeiro (7 million inhabitants), and 220 km from the city of São Paulo (12 million inhabitants). The nuclear power plants occupy a coastal area called “Praia de Itaorna” (Itaorna Beach). The Highway BR-101 traverses the region at an average of 200 m north of the NPP site limits.

The study area presents a typical microclimate regime of a tropical coastal region, influenced by factors like latitude, longitude, the proximity of the ocean, relief, nature of the vegetation cover, and, in particular, the action of atmospheric circulation systems in large and mid-scales, such as cold fronts and sea/land wind regimes. The site has a humid tropical climate, with an average annual rainfall of 1817 mm, with maximum rainfall occurring mainly from October to March, and an average annual temperature of 21.4 °C (data from 1982 to 2001, according to Eletronuclear 2005). The Köppen Climate Classification subtype for this climate is “Cfa”. (Humid Subtropical Climate).

In general terms, the geomorphology of the place is characterized to the north by elevated terrains, constituted by the hills and escarpments of the Serra do Mar mountain range. To the south, occurs the fluvio-marine coastal plain, in the coves and beaches. The main hydrological pattern consists of rivers and streams that have their springs at the hillsides of the Serra do Mar and flow downhill towards the coastal plains and beaches. The Mambucaba River (Fig. 1) is the primary watercourse in the study area.

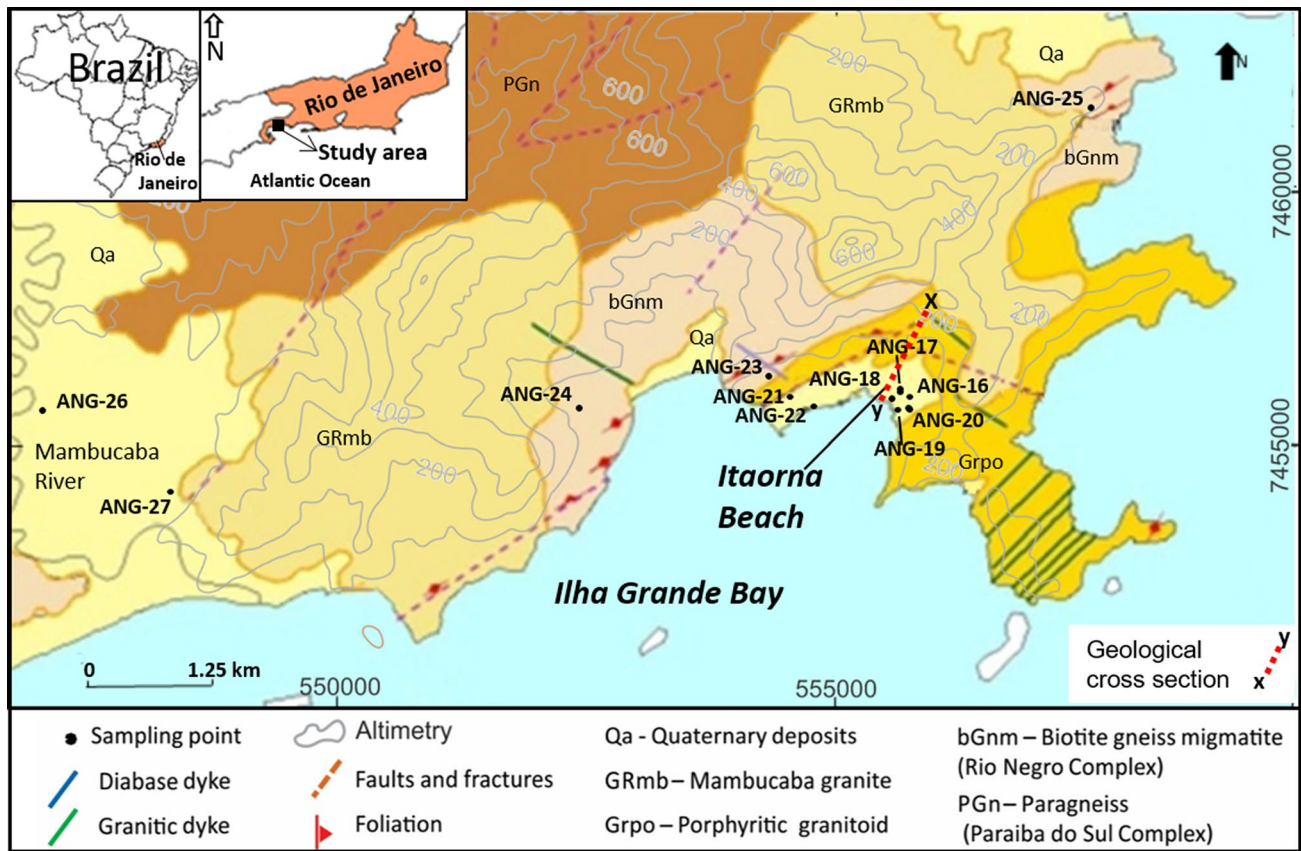


Fig. 1 Location and Geological map of the study area showing water sampling points. Modified from Eletronuclear (2005)

### Geological and hydrogeological conceptual model

The study area has been the subject of hydrogeological and geological studies in the last 20 years, mainly due to surveys for licensing of nuclear power plants, as UFRJ (2003) and Eletronuclear (2005), among others. Figure 1 shows a geological map of the study area. A geological and hydrogeological schematic cross-section is shown in Fig. 2. The crystalline basement comprises granite–gneissic proterozoic rocks belonging to the Paraíba do Sul and Rio Novo Complexes (Eletronuclear 2005; CPRM 2007). These rocks are characterized by the predominance of garnet–biotite gneisses, hornblende–biotite gneisses, migmatites, and kinzigites. Porphyritic granitoid bodies containing microcline, oligoclase, quartz, and biotite occur embedded in the orthogneisses of the Rio Novo Complex. This Neoproterozoic unit has outcrops at NPP’s site at Itaorna Beach. The Cambro-Ordovician Mambucaba Granite, mainly composed of oligoclase, biotite, and quartz, is located in the region of Mambucaba (east of the homonymous river plain) with outcrops at Itaorna Beach. It consists of small stocks and clusters of intrusive dykes in the rocks of the Rio Novo Complex. Expressive systems of basic (tholeiitic) rock dykes of

Mesozoic age (Guedes et al. 2005) are observed in the study area, including Itaorna Beach (Eletronuclear 2005; CPRM 2007). These dykes have hydrogeological importance as they are preferably lodged along with pre-existing fractures and have internal orthogonal joint systems, which can store and conduct water.

The quaternary units are represented by alluvial deposits associated with the present-day and ancient drainage network, consisting of gravel, fine and medium sand, silt, and clay, including the deposits of terraces and floodplains. Fluvial–marine and marine deposits are also present, constituted by present-day and older sediments, representing deposits of the continental–marine transition environment to essentially marine. Fluvial–marine and marine sediments generally consist of layers of fine, medium, and coarse sand, alternated by levels of clay and silt, formed due to successive oscillations in sea level (Eletronuclear 2005).

The hillsides close to the NPP’s site present colluvial and talus deposits, consisting of soils with a brownish, sandy, micaceous texture, with several blocks and boulders rolled in the soil matrix and intense vegetation. The intense cracking of the rocks causes numerous water springs at the foot of the hillsides next to the bed of the BR-101 highway (Eletronuclear 2005). There are mangrove deposits at the

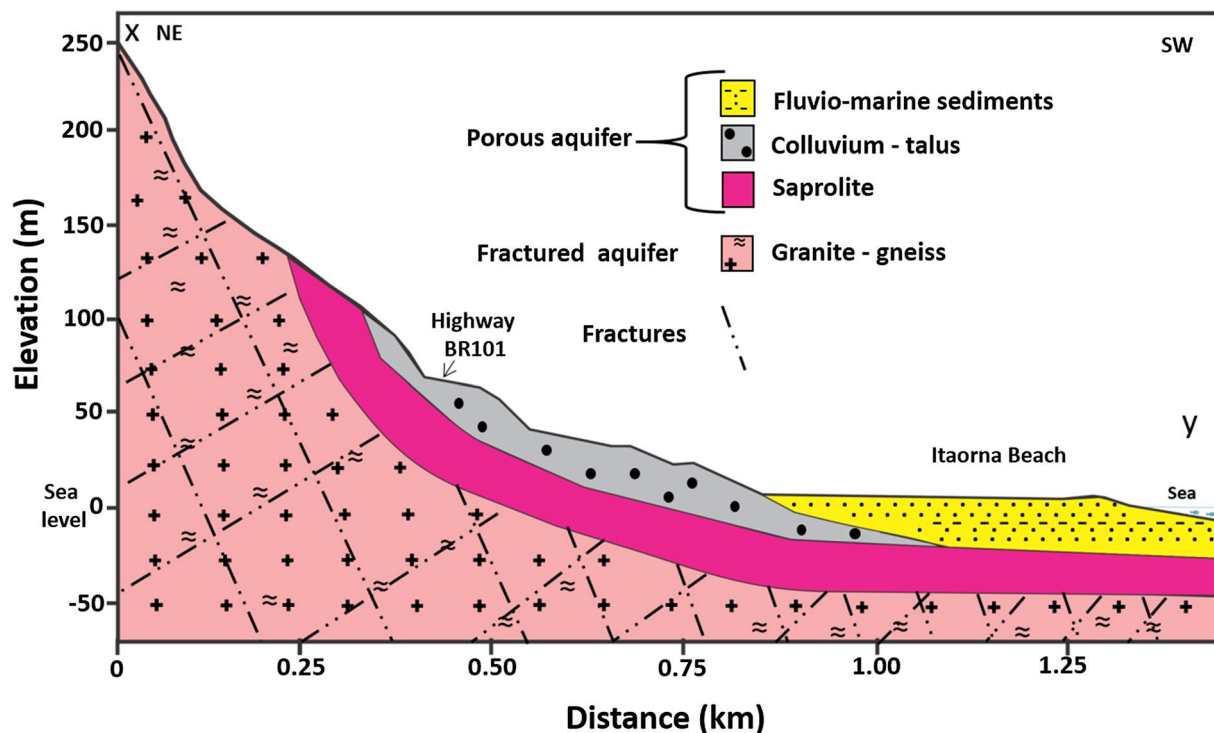


**Fig. 2** Geological and hydrogeological schematic cross-section  $x$ - $y$  (see Fig. 1). The elevation and distance values are approximate, as well as the thickness of the lithotypes

mouth of some rivers, characterized by silt-clayey muds and sludge rich in organic matter, dark in color, characteristically formed in a reducing environment derived from the decomposition of plant remains. Generally, the gneisses show local and regional schistosity and around  $N 50^{\circ}$  to  $70^{\circ}$  E, with high dip angles,  $60^{\circ}$  to  $80^{\circ}$  NW. Two fracture directions are dominant in the area: NE and NNW.

Two main types of aquifers can be found in the region (Eletronuclear 2005). The first one is a free, porous, and shallow aquifer type (upper aquifer). The other is a fractured semi-confined type, characterized by fractures of crystalline rocks (Fig. 2). The unconfined and porous aquifer (0 to 40 m deep) occurs in the lowlands, river, and coastal plains; it is represented by the river and marine river sediments, composed in its upper portion by sandy sediments (locally silt-rich), containing fragments of seashells. These fluvial-marine sediments occur over a sandy-clayey saprolite, containing fragments of the fresh rock and pebbles (eventually boulders) resulting from the weathering of the granitic-gneiss basement, forming the basis of the porous aquifer. In the NPP's facilities area, this aquifer is commonly covered by a layer of landscaping material. On the hillsides, this aquifer is represented by the saturated portions of the talus and colluvium deposits, residual soil, and saprolite.

Locally, the fluvial-marine sediments are interspersed with layers of clay, one of which, of greater thickness

(1–10 m thickness) and lateral continuity, is constituted by organic, dark, and plastic clay, presenting fragments of shells, and that mainly occurs over the saprolite. This clay layer must result from sea-level fluctuations, frequent in the quaternary (Martin et al. 1996). Due to the absence of more boreholes and piezometers, the lateral continuity of this clay layer can only be confirmed in the vicinity of the NPP's facilities. Undoubtedly, it is a clay aquifuge or aquitard that, when present, could be acting as a confining layer for the groundwater below. According to Eletronuclear (2005), this porous aquifer is in hydraulic connection with the superficial portions of the fractured aquifer.

The fractured and semi-confined aquifer (0 to undefined m deep) is represented by the fracture network of the crystalline basement rocks. It occurs both on the surface (outcrops) and in-depth under the porous aquifer. According to Eletronuclear (2005), the gradients and the hydraulic load are high, as the recharge is frequently at the top of the hillsides (up to 500 m high) located north of the NPP's site. This aquifer is unconfined in the elevated portions of the hillsides, occupied by extensive outcrops of the crystalline basement. It becomes confined under the layers of saprolite and colluvium/talus deposits and the fluvial-marine deposits in the coastal region. Sometimes, this aquifer has its piezometric level at or above the land surface (Eletronuclear 2005). This fractured aquifer in granitic-gneiss crystalline rocks is very

common in the coastal region of southeastern Brazil, with the recharge areas located in the highest parts of the hills (Silva-Filho et al. 2009).

Previous hydrogeochemistry studies at the NPP's site (UFRJ 2003; Eletronuclear 2005) identified three distinct groups of waters: Group I: Na-Cl water type, with a subgroup of these waters in which the concentration of calcium was slightly greater: Ca-Na-Cl- water type; Group II, waters from the deep tubular wells: Ca-Na-HCO<sub>3</sub>-Cl water type and Group III: Ca-HCO<sub>3</sub> water type. Regarding the groundwater flow, its direction is mainly from NNE to SSW and discharging into the ocean at the Itaorna Bay, which agrees with the ground surface topography. The water table is about 2 m below the ground surface, with a slope of 0.5% towards the ocean (Eletronuclear 2005).

## Methodology

Twelve water samples were collected in October 2018 (Fig. 1 and Table 1) to obtain the hydrochemical data. Eight samples (ANG-16 to ANG-23) were collected from piezometers used for monitoring purposes (8–10 m deep) and located at the NPP's site, on Itaorna beach. The water samples from the piezometers were obtained with a low flow pumping system. The ANG-24 and ANG-25 samples were collected on the hillside close to the NPP's site: the first comes from a small dam, close to a water treatment station (EPTA); the second comes from a groundwater spring. For the Mambucaba River Plain, sampling (ANG-26 and ANG-27) was carried out from two shallow wells (4–8 m deep), used for domestic purposes. In these wells, water samples were collected directly from the pumps installed in them, after repeated purges of the wells until the stability of electrical conductivity, to ensure that the samples will represent the groundwater.

Electrical conductivity (EC), total dissolved solids (TDS), redox potential (Eh), temperature (T), and pH were measured in situ using an Ultrameter II multiparameter handheld meter (Myron L Company). The water samples were collected in properly clean polyethylene bottles (250–500 mL). They were filtered through 0.45 µm membranes, and the samples for cation analyses were acidified with HNO<sub>3</sub> (pH < 2) to stop bacterial growth and metal oxidation (Appelo and Postma 2005). The bottles were placed in thermally insulated boxes (± 4 °C) and then taken to the laboratory.

The analytical determinations carried out were as follows: alkalinity (titration); cations Ca<sup>2+</sup> and Mg<sup>2+</sup> (atomic absorption/spectrometry); cations Na<sup>+</sup> and K<sup>+</sup> (liquid chromatography); anions, Cl<sup>-</sup> and SO<sub>4</sub><sup>2-</sup> (liquid chromatography); Si (Inductively coupled plasma mass spectrometry—ICP-MS). The detection limits (DL) for individual elements were 0.1 mg/L for anions and 0.05 mg/L for cations. All

these analyses were performed at the Nuclear Technology Development Center (CDTN/Brazil). The hydrochemical data were evaluated through diagrams and scatter plots. The reliability of the chemical analyses was evaluated according to the acceptance criteria proposed by APHA (1999), using the following formula:

$$\% \text{difference} = 100 \frac{(\sum \text{cation} - \sum \text{anions})}{(\sum \text{cation} + \sum \text{anions})} \quad (1)$$

The global mean composition for seawater estimated by Millero (2013) was used as a reference value. It was also used as reference data the ionic composition of rainwater (volume-weighted average—VWA) determined by Souza et al. (2006) in rain samples collected at Ilha Grande, which is an island about 20 km offshore from Itaorna beach (Fig. 1). As the direct analysis of alkalinity was not done by Souza et al. (2006), the concentration of bicarbonate (HCO<sub>3</sub><sup>-</sup>) ion was estimated from pH and atmospheric CO<sub>2</sub> partial pressure, assuming gas–liquid equilibrium (Brimblecombe 1986; Tiwari et al. 2012), using the equation

$$[\text{HCO}_3^-] = K_H K_1 p\text{CO}_2 / [\text{H}^+], \quad (2)$$

where  $K_H$  Henry's law constant for CO<sub>2</sub> solubility = 3.4 × 10<sup>4</sup> µeq/L atm<sup>-1</sup>;  $K_1$  First dissociation constant for H<sub>2</sub>CO<sub>3</sub> = 4.5 × 10<sup>-1</sup> µeq/LpCO<sub>2</sub>; Partial pressure of CO<sub>2</sub> = 3.87 × 10<sup>-4</sup> atm.

## Results and discussion

### General hydrogeochemistry

Descriptive statistics (Table 1), considering all data, shows a significant variation in parameter values, resulting in high standard deviation (SD) values. Certainly, this is related to considering both continental water and waters with higher influence from the sea. The total dissolved solids (TDS) varied from 13 to 21,130 mg/L, with a mean value of 1900 mg/L (median value of 155 mg/L). The pH ranged from acidic (5.4) to alkaline (7.9) with a neutral mean/median value (7.0). Considering the mean value, the abundance of the major ions is as follows: Na<sup>+</sup> > Mg<sup>2+</sup> > Ca<sup>2+</sup> > K<sup>+</sup> and Cl<sup>-</sup> > HCO<sub>3</sub><sup>-</sup> > SO<sub>4</sub><sup>2-</sup>. However, this analysis considering all samples must be carefully interpreted, as the extreme values measured in the Group 4 sample (ANG-22), with strong interference from the seawater, as we will see later, caused a large standard deviation in all parameters. Therefore, considering the more appropriate median values, the abundance of the major ions is as follows: Ca<sup>2+</sup> > Na<sup>+</sup> > K<sup>+</sup> > Mg<sup>2+</sup> and HCO<sub>3</sub><sup>-</sup> > Cl<sup>-</sup> > SO<sub>4</sub><sup>2-</sup>. The groups and their statistical data will be considered later when the water types are discussed. Regarding the seawater (Millero 2013), the TDS is

**Table 1** Descriptive summary of the hydrogeochemical parameters considering all the water samples and by water type group

| Group       | Statistic | Temp (°C) | Eh (mV) | EC (µS/cm) | TDS (mg/L) | pH (-) | HCO <sub>3</sub> <sup>-</sup> (mg/L) | Cl <sup>-</sup> (mg/L) | SO <sub>4</sub> <sup>2-</sup> (mg/L) | K <sup>+</sup> (mg/L) | Na <sup>+</sup> (mg/L) | Mg <sup>2+</sup> (mg/L) | Ca <sup>2+</sup> (mg/L) | SiO <sub>2</sub> (mg/L) |
|-------------|-----------|-----------|---------|------------|------------|--------|--------------------------------------|------------------------|--------------------------------------|-----------------------|------------------------|-------------------------|-------------------------|-------------------------|
| All (N=12)  | Minimum   | 20.6      | 79      | 23         | 13         | 5.4    | 11                                   | 2.3                    | 0.9                                  | 0.8                   | 2.6                    | 0.3                     | 0.6                     | 6.4                     |
|             | Maximum   | 28.4      | 494     | 23,190     | 21,130     | 7.9    | 357                                  | 8167.9                 | 1200.4                               | 164.4                 | 4388.2                 | 490.0                   | 211.0                   | 16.5                    |
|             | Median    | 24.2      | 268     | 257        | 155        | 7.0    | 134                                  | 6.2                    | 5.6                                  | 3.5                   | 7.3                    | 2.5                     | 31.5                    | 8.5                     |
|             | Mean      | 24.7      | 273     | 2161       | 1900       | 7.0    | 134                                  | 688.2                  | 105.3                                | 18.6                  | 377.2                  | 46.0                    | 40.3                    | 9.5                     |
|             | SD        | 2.4       | 133     | 6625       | 6057       | 0.9    | 108                                  | 2355.5                 | 344.9                                | 46.2                  | 1263.2                 | 140.0                   | 57.3                    | 3.1                     |
| 1 (N=3)     | Minimum   | 20.6      | 237     | 23         | 13         | 5.4    | 11                                   | 2.3                    | 0.9                                  | 0.8                   | 2.6                    | 0.3                     | 0.6                     | 11.8                    |
|             | Maximum   | 22.7      | 494     | 88         | 52         | 6.8    | 32                                   | 6.9                    | 1.3                                  | 1.3                   | 5.4                    | 0.8                     | 1.9                     | 16.5                    |
|             | Median    | 22.3      | 405     | 33         | 20         | 5.9    | 11                                   | 3.7                    | 1.0                                  | 1.2                   | 3.2                    | 0.6                     | 1.6                     | 13.9                    |
|             | Mean      | 21.9      | 379     | 48         | 28         | 6.0    | 18                                   | 4.3                    | 1.1                                  | 1.1                   | 3.7                    | 0.6                     | 1.4                     | 14.1                    |
|             | SD        | 1.1       | 131     | 35         | 21         | 0.7    | 12                                   | 2.3                    | 0.2                                  | 0.2                   | 1.5                    | 0.2                     | 0.7                     | 2.3                     |
| 2 (N=6)     | Minimum   | 23.5      | 79      | 200        | 120        | 6.8    | 99                                   | 3.9                    | 3.2                                  | 3.3                   | 4.7                    | 1.2                     | 25.0                    | 6.4                     |
|             | Maximum   | 28.4      | 390     | 666        | 417        | 7.9    | 357                                  | 28.1                   | 9.3                                  | 15.8                  | 53.3                   | 23.0                    | 52.0                    | 9.5                     |
|             | Median    | 26.9      | 173     | 358        | 220        | 7.7    | 190                                  | 8.1                    | 5.6                                  | 7.2                   | 13.7                   | 9.2                     | 43.0                    | 7.5                     |
|             | Mean      | 26.4      | 195     | 384        | 236        | 7.5    | 207                                  | 11.2                   | 5.8                                  | 8.2                   | 18.7                   | 9.6                     | 41.7                    | 7.8                     |
|             | SD        | 2.1       | 121     | 155        | 99         | 0.4    | 86                                   | 9.1                    | 2.3                                  | 5.0                   | 18.3                   | 7.7                     | 9.6                     | 1.3                     |
| 3 (N=2)     | Minimum   | 24.0      | 270     | 125        | 74         | 6.0    | 42                                   | 4.8                    | 10.2                                 | 2.6                   | 6.8                    | 1.1                     | 7.9                     | 7.7                     |
|             | Maximum   | 24.8      | 304     | 169        | 100        | 6.6    | 58                                   | 6.4                    | 14.5                                 | 3.0                   | 8.8                    | 1.8                     | 11.0                    | 9.7                     |
|             | Median    | 24.4      | 287     | 147        | 87         | 6.3    | 50                                   | 5.6                    | 12.4                                 | 2.8                   | 7.8                    | 1.5                     | 9.5                     | 8.7                     |
|             | Mean      | 24.1      | 295     | 155        | 99         | 6.3    | 50                                   | 5.6                    | 12.4                                 | 2.8                   | 7.8                    | 1.5                     | 9.5                     | 8.7                     |
|             | SD        | 0.6       | 24      | 31         | 18         | 0.4    | 11                                   | 1.1                    | 3.0                                  | 0.3                   | 1.4                    | 0.5                     | 2.2                     | 1.4                     |
| 4 (N=1)     | value     | 24.1      | 395     | 23,190     | 21,130     | 7.6    | 210                                  | 8167.9                 | 1200.4                               | 164.4                 | 4388.2                 | 490.0                   | 211.0                   | 7.6                     |
|             | Seawater* | -         | -       | -          | 35,046     | 8.1    | 105                                  | 19,352.7               | 2712.4                               | 399.1                 | 10,781.5               | 1283.7                  | 412.1                   | -                       |
| Rainwater** | -         | -         | -       | 13         | 13         | 5.2    | 0.1                                  | 6.3                    | 1.7                                  | 0.3                   | 3.3                    | 0.5                     | 0.2                     | -                       |

- Not available

\*Global mean composition for seawater estimated by Millero (2013)

\*\*Ionic composition of rainwater determined by Souza et al. (2006) at Ilha Grande

35046 mg/L (very high), the pH is a slightly alkaline 8.1, and the major concentration rank is:  $\text{Na}^+ > \text{Mg}^{2+} > \text{Ca}^{2+} > \text{K}^+$  and  $\text{Cl}^- > \text{SO}_4^{2-} > \text{HCO}_3^-$ . In relation to seawater, the rainwater (Souza et al. 2006) is expect to be more acidic,  $\text{pH} = 5.22$ , less mineralized,  $\text{TDS} = 13.17 \text{ mg/L}$ , and with a similar ionic abundance rank:  $\text{Na}^+ > \text{Mg}^{2+} > \text{K}^+ > \text{Ca}^{2+}$  and  $\text{Cl}^- > \text{SO}_4^{2-} > \text{HCO}_3^-$ .

**Water types**

Based on the Piper diagram (Piper 1944), the waters under investigation can be classified into four major groups (Fig. 3):

**Group 1 Ca–Na–HCO<sub>3</sub> waters type**

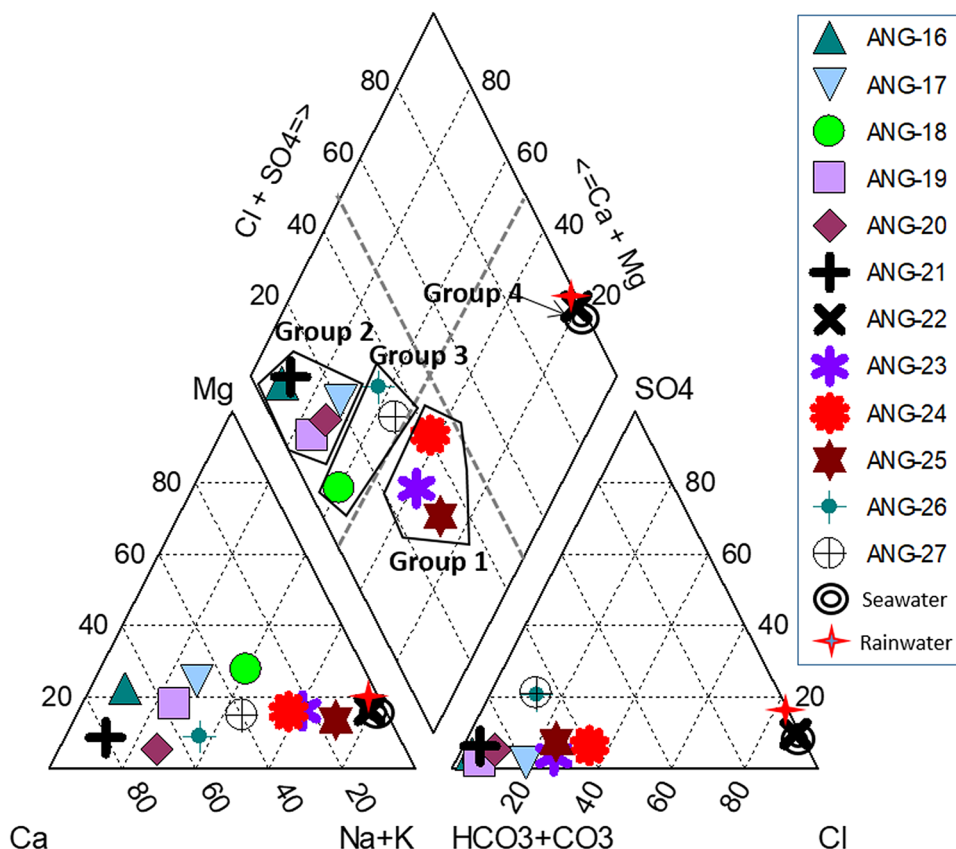
It is represented by a groundwater sample (ANG-23), a sample from a small reservoir (ANG-24), and a sample from a groundwater spring (ANG-25). These samples were collected in the hillside environment, where predominate granitic–gneissic basement outcrops, residual soil, talus deposits, and dense vegetation, representing an aquifer recharge zone, but with occurrences of discharge points from the fractured aquifer. Compared to the other groups (Table 1), the waters in this group are the least mineralized, with an average TDS of 28 mg/L and ranging from

13 to 52 mg/L. The lowest TDS value is similar to the value measured by Souza et al. (2006) in regional rainwater, 13. As well, the minimum pH value, 5.4, is similar to that found by this author in rainwater, 5.2. The average pH is 6.0, and the maximum is 6.8. Considering the mean value, the abundance of the major ions is as follows:  $\text{Na}^+ > \text{Ca}^{2+} > \text{K}^+ > \text{Mg}^{2+}$  and  $\text{HCO}_3^- > \text{Cl}^- > \text{SO}_4^{2-}$ . Especially noteworthy is the high silica content of this group compared to the others.

**Group 2 Ca–HCO<sub>3</sub> waters type**

It is represented by samples ANG-16, ANG-17, ANG-18, ANG-19, ANG-20, and ANG-21. These are all groundwater samples collected at Itaorna Beach, close to the current and future NPP facilities. These samples come from the porous aquifer and seem to correspond to group 3, individualized in previous hydrogeological surveys carried out in the study area by UFRJ (2003) and Eletronuclear (2005). As shown in Table 1, the pH range is 6.8–7.9 (neutral to alkaline) with an average value of 7.5. The TDS range is 120–417 mg/L with an average value of 236 mg/L. These values indicate more mineralized and alkaline waters than those in Group 1. The major ions abundance is as follows:  $\text{Ca}^{2+} > \text{Na}^+ > \text{Mg}^{2+} > \text{K}^+$  and  $\text{HCO}_3^- > \text{Cl}^- > \text{SO}_4^{2-}$

**Fig. 3** Piper diagram of the waters from the study area. The seawater from Millero (2013) and the rainwater from Souza et al. (2006)



### Group 3 Ca–(Na)–HCO<sub>3</sub> waters type

According to Piper Diagram, this group could be classified as a sub-group of Group 2. However, considering the Chadha Diagram (Chadha 1999, Fig. 3) and other geochemical plots shown later, it is better to consider it a separate group. This group seems to represent a mixture or an intermediate stage (flow and chemical composition) between the waters of groups 1 and 2. It is represented by two samples (ANG-26 and ANG-27) of groundwater collected in the Mambucaba River plain (Fig. 1). These samples were collected from the sandy porous aquifer on a coastal plain where ancient and current fluvial and marine sediments occur. The TDS values vary in an intermediate range between Groups 1 and 3, 74–100 mg/L (mean = 87 mg/L), and pH more similar to Group 1. The ionic abundance is as follows:  $\text{Ca}^{2+} \approx \text{Na}^+ > \text{K}^+ > \text{Mg}^{2+}$  and  $\text{HCO}_3^- > \text{Cl}^- > \text{SO}_4^{2-}$

### Group 4 Na–Cl waters type

One sample (ANG-22) is represented, bearing an ionic composition typical of high seawater influence: It has the highest values for TDS (21,130 mg/L) and ions, and presents the following rank in terms of ionic abundance (like the seawater):  $\text{Na}^+ > \text{Mg}^{2+} > \text{Ca}^{2+} > \text{K}^+$  and  $\text{Cl}^- > \text{SO}_4^{2-} > \text{HCO}_3^-$ . This group corresponds to group 1 defined by the previous research (UFRJ 2003; Eletronuclear 2005).

The sample data were plotted in the Chadha diagram (Chadha 1999) to identify the different types of water. In this diagram (Fig. 4), the X-axis represents the difference between  $(\text{Ca}^{2+} + \text{Mg}^{2+})$  and  $(\text{Na}^+ + \text{K}^+)$  in meq/L %, and

the Y-axis represents the difference between  $(\text{HCO}_3^-)$  and  $(\text{Cl}^- + \text{SO}_4^{2-})$  in meq/L %. The four water types suggested by Chadha (1999) are shown in the quadrants of Fig. 4. It is found that the Group 1 samples fell in the Na–HCO<sub>3</sub> type quadrant and the Group 2 samples fell in the Ca–HCO<sub>3</sub> type quadrant, as noted in Piper's diagram. The Group 3 samples fell into the Ca–HCO<sub>3</sub> type, but they can be considered an intermediate group: with less Ca than Group 1 and less Na than Group 2, as proposed in the analysis of Piper's diagram (Fig. 3). The Group 4 sample fell in the Na–Cl type quadrant, very close to the global mean value for seawater (Millero 2013), clearly indicating seawater interference. Similarly, elevated concentrations of  $\text{Cl}^-$  and  $\text{Na}^+$  were observed in a Mediterranean coastal area in Greece, near the coastline, indicating a zone of seawater intrusion (Papazotos et al. 2019). In the Zhang and Zhang (2021) study in an alluvial fan, Japan, the hydrological connection between fresh submarine groundwater and the coastal confined groundwater was observed, in which there was a high salinity beneath the clay layer as a result of freshwater–seawater mixing. According to Khan et al. (2021), salinity caused by the seawater influence is one of the significant threats for coastal aquifers systems in the world and can be induced by variations in the sea level, low infiltration of freshwater, excess withdrawal of coastal groundwater, etc. In the work of Rajaveni et al. (2021), a calibrated and integrated density-dependent groundwater model in the FEFLOW platform was used to investigate the best management options to mitigate the seawater intrusion by different scenarios in a multi-layered coastal aquifer. Scenarios such as the construction of additional check dams, increase in crest level of existing check

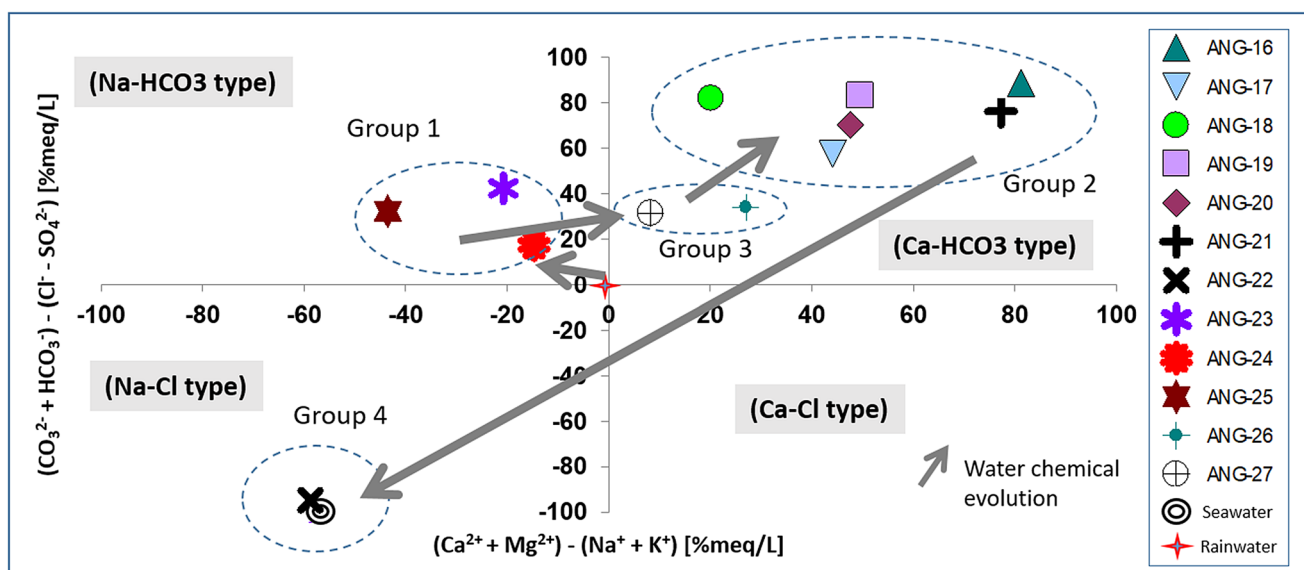


**Fig. 4** Chadha's diagram of the waters from the study area. The dashed circles indicate the water groups. The seawater values from Millero (2013) and the rainwater values from Souza et al. (2006)



dam, rejuvenation and cleaning of defunct water bodies, and termination of pumping were assessed and considered to help to dissolve salinity concentration and desalinizes groundwater for about 5 km. In this study, a piezometer was installed very close to the coastline and is subject to the fluctuation of the ocean tides.

Considering the elevation of the samples (Figs. 1 and 2) and the Chadha diagram (Fig. 4), it can be interpreted that starting from the recharge zone (hills and flat hillsides) towards the coastal zone, the sodium bicarbonate waters (Group 1) will enrich themselves in calcium (Groups 3 and 2), and at a certain point, they start to be influenced by seawater (Group 4).

The pH versus TDS (mg/l) scatter plot (Fig. 5) brings some information that confirms the observations made so far about groups, types of water, and direction of flow. It is observed in this plot that Group 1 has a pH ranging from 5.6 to 6.8 and the TDS < 70 mg/L. In relative terms, it is the group with the lowest pH and TDS values; thus, they are the most acidic and least mineralized waters. This behavior is undoubtedly related to the fact that they are waters from the recharge zone or have a short residence time in contact with the aquifers lithologies.

Showing pH and TDS (Fig. 5) values of 6.0–6.5 and 70–100 mg/L, respectively, are the samples from Group 3, which are clearly in an intermediate position between Group 1 and Group 2, in terms of H<sup>+</sup> concentration and dissolved ions. Group 2 fell in a range with pH 6.8–8.0 and

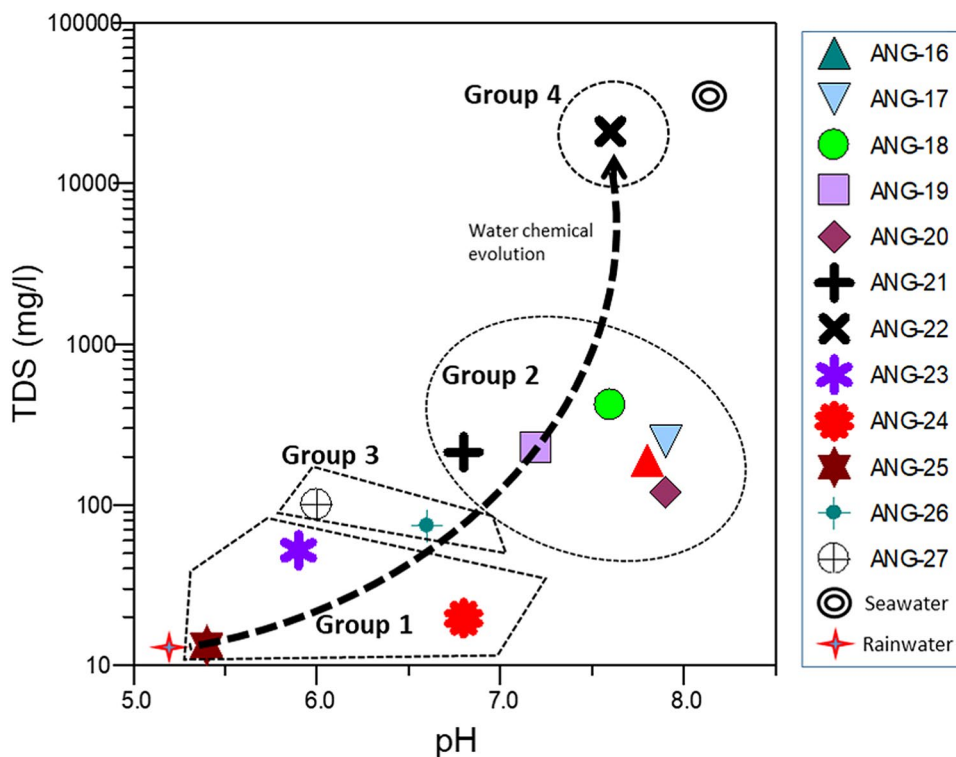
TDS between 100 and 1000 mg/L, more mineralized and alkaline than the samples of Group 1 and Group 3. Both aspects suggest the influence of carbonate weathering in the waters of Group 2, following the porous marine sedimentary aquifer characteristics. Group 4 presents a very high TDS value (21,130 mg/L): one more indication of seawater interference, while the alkaline pH value indicates weathering of the carbonate terms of the porous coastal aquifer.

### Hydrochemical processes

The Gibbs diagram (Fig. 6, Gibbs 1970) has been widely used as a first approach for understanding the relative importance of the significant natural processes that control and determine the composition of groundwater (Tiwari et al. 2019; Sefie et al. 2018; Nandakumaran and Balakrishnan 2020; Khan et al. 2021; Madhav et al. 2021; Zeng et al. 2021). It depicts log TDS against the ratios of cations Na<sup>+</sup>/(Na<sup>+</sup> + Ca<sup>2+</sup>) and the ratio of anions Cl<sup>-</sup>/(Cl<sup>-</sup> + HCO<sub>3</sub><sup>-</sup>), and defines three main zones: evaporation, rainfall, and rock dominance.

The ANG-22 sample (Group 4) fell in the evaporation domain, which is one more indication of the seawater influence in this sample. Most of the samples (Group 2) fell into the rock dominance zone, which indicates that the rock–water interactions are the main factor that controls the chemical composition of these samples. Group 1 samples (ANG-23, ANG-24, and ANG-25) are in the zone of the rainfall domain. This

**Fig. 5** Scatter plot of TDS (mg/L) versus pH for samples of the study area. The Seawater values from Millero (2013) and the rainwater values from Souza et al. (2006)



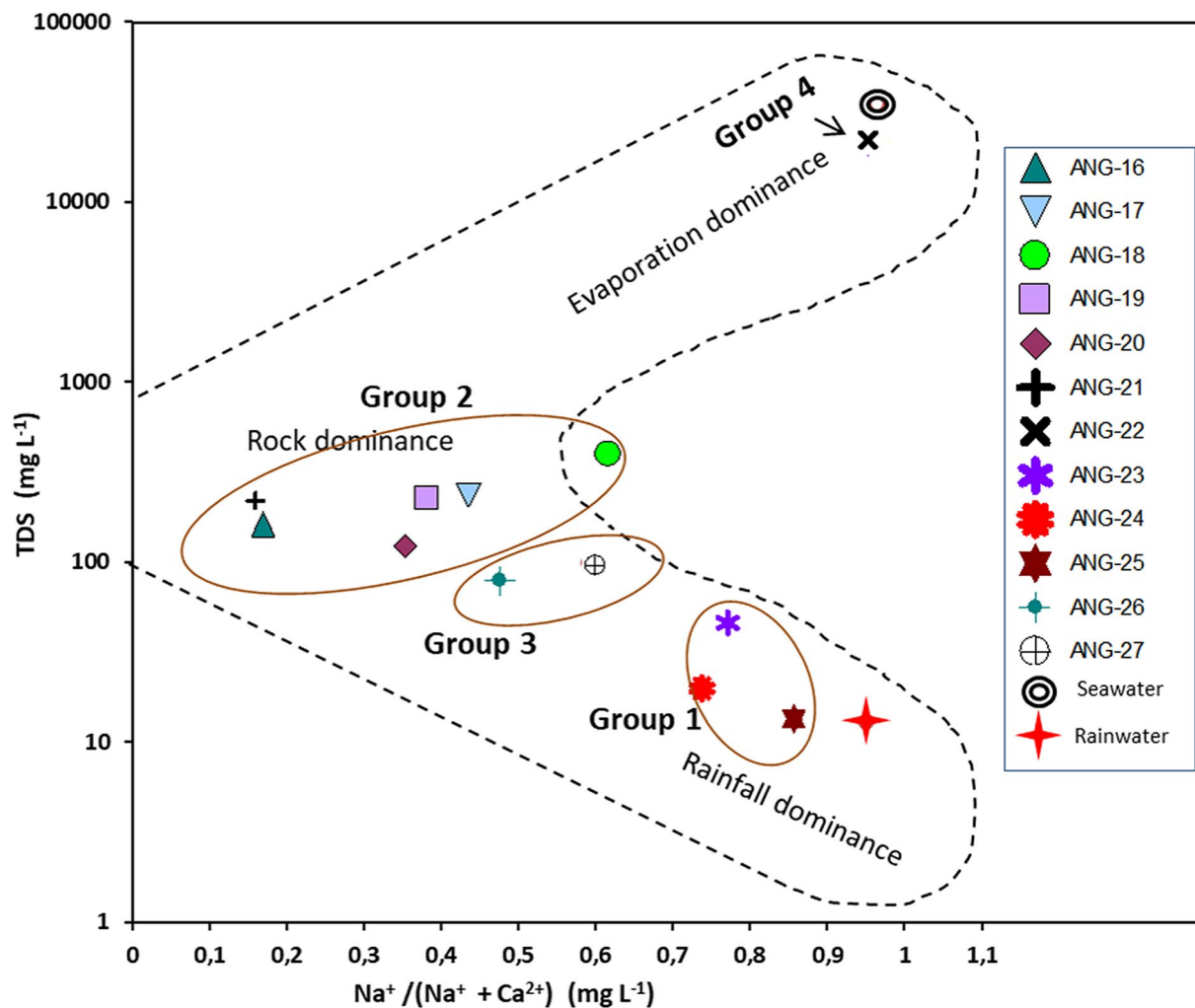
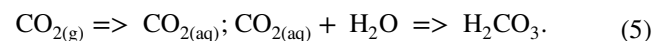
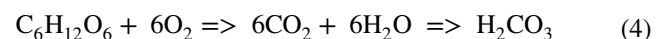
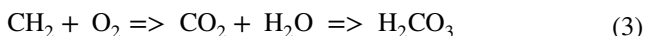


**Fig. 6** Gibbs diagrams, considering cations, of the study area samples. TDS vs.  $\text{Na}^+ / (\text{Na}^+ + \text{Ca}^{2+})$ . The Seawater values from Millero (2013) and the rainwater values from Souza et al. (2006)

suggests that although these samples must suffer some influence from the weathering of the rocks (mainly ANG-23), they have contact with the atmosphere, mainly concerning ANG-24 (spring area) and ANG-25 (surface water). The fact that these three samples are influenced by precipitation is consistent with how they occur on the slopes in places with crystalline rocks outcrops, residual soils, talus deposits, and denser vegetation (Fig. 1) and this also explains the low mineralization of these waters and the more acidic pH (Fig. 5). This acidification was likely due to one of the following factors, or their combination: organic matter decomposition (reaction 3), respiration of plants (reaction 4), and the natural pH of uncontaminated rainwater in the atmosphere, 5.5–6.0 (reaction 5) (Hounslow 1995; Appelo and Postma 2005)

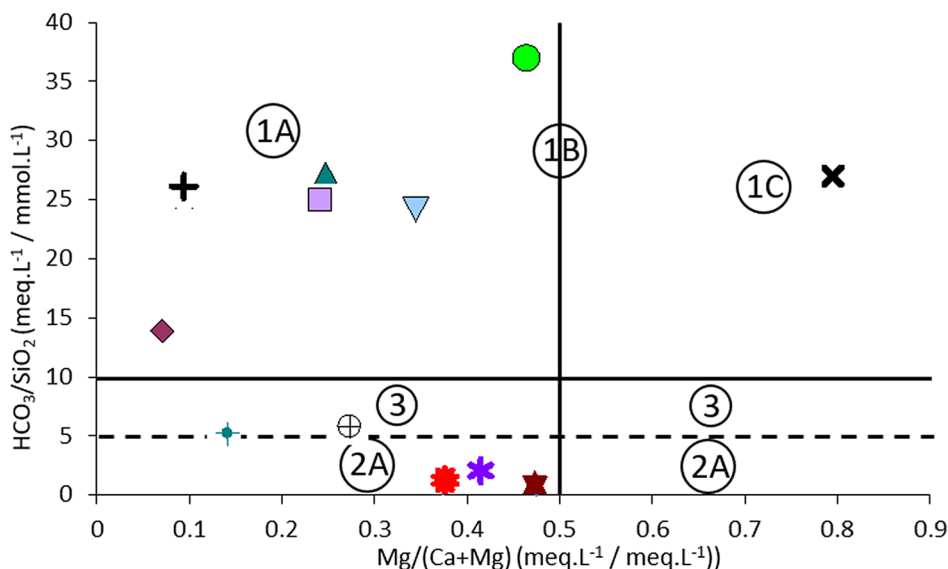


It is observed (Fig. 6) that the samples ANG-26 and ANG-27 (Group 3) are in an intermediate position between rock dominance (Group 2) and rainfall dominance (Group 1) zones. This suggests that they are water resulting from the mixture of these two groups and/or that depicts an intermediate step in the chemical evolution of the waters of the study area, departing from Group 1, less mineralized waters, to Group 2, with more significant rock–water interaction.

#### Scatter plot $\text{HCO}_3^- / \text{SiO}_2$ ratio versus $\text{Mg}^{2+} / (\text{Ca}^{2+} + \text{Mg}^{2+})$ ratio

The scatter plot in Fig. 7 was prepared based on Hounslow (1995) and aimed to indicate the type of rock with which the

**Fig. 7** Scatter plot of  $\text{HCO}_3^-/\text{SiO}_2$  ratio versus  $\text{Mg}^{2+}/(\text{Ca}^{2+}+\text{Mg}^{2+})$  molar ratio. Adapted from Hounslow (1995)



|  |    |  |   |
|--|----|--|---|
| $\text{HCO}_3^-/\text{SiO}_2 > 10$ (Not silicate weathering) |    | <ul style="list-style-type: none"> <li><span style="color: green;">▲</span> ANG-16</li> <li><span style="color: blue;">▼</span> ANG-17</li> <li><span style="color: green;">●</span> ANG-18</li> <li><span style="color: purple;">■</span> ANG-19</li> <li><span style="color: brown;">◆</span> ANG-20</li> <li><span style="color: black;">+</span> ANG-21</li> <li><span style="color: black;">×</span> ANG-22</li> <li><span style="color: purple;">✱</span> ANG-23</li> <li><span style="color: red;">✱</span> ANG-24</li> </ul> | <ul style="list-style-type: none"> <li><span style="color: red;">★</span> ANG-25</li> <li><span style="color: teal;">⊕</span> ANG-26</li> <li><span style="color: grey;">⊕</span> ANG-27</li> </ul> |
| $\text{Mg}/\text{Ca}+\text{Mg}$                              | ①A | $< 0.5$ (Calcite-dolomite weathering)  |   |
|  | ①B | $= 0.5$ (Dolomite weathering)  |   |
|  | ①C | $> 0.5$ (Seawater)   |   |
| $\text{HCO}_3^-/\text{SiO}_2 < 5$ (Silicate weathering)      |    |  |   |
| $\text{Mg}/\text{Ca}+\text{Mg}$                              | ②A | $< 0.5$ (Granitic weathering)  |   |
|  | ②B | $> 0.5$ (Ferromagnesian minerals)  |   |
| ③  |    | $5 < \text{HCO}_3^-/\text{SiO}_2 < 10$ (Ambiguous)   |   |

water interacted when passing through pores and/or fractures. It can be seen in this figure that the samples ANG-16 to ANG-21 (Group 2) fell in area 1A, indicating that their composition is predominantly related to the “Not silicate weathering” and, more specifically, to the weathering of carbonate rocks (calcite–dolomite minerals). The ANG-22 sample (Group 4) is also related to the weathering of non-silicate rocks but fell in area 1C, indicating seawater interference. These observations made for Groups 2 and 4 are in line with the characteristics defined previously for the porous fluvial–marine aquifer of the coastal region, locally with interference from seawater.  $\text{Ca}^{2+}/\text{Mg}^{2+}$  ratio (median values) is increasing from Group 1 (2.8) to Group 2 (4.7) to Group 3 (6.5), suggesting that carbonate weathering is the main cause of Ca in groundwater (Madhav et al. 2021).

The samples ANG-23 to ANG-25 (Group 1) are in area 2A, suggesting waters with chemical composition influenced by the weathering of silicates, and more specifically, granite composition rocks. This behavior is consistent, since these samples were collected on the hills where the fractured

aquifer of granitic-gneisses composition outcrops, and therefore, its chemical weathering products are present. Rock-water interaction and silicate weathering are common factors that affect groundwater in these conditions (Bodrud-Doza et al. 2019; Khan et al. 2021). The ANG-26 and ANG-27 (Group 3) samples are positioned on or slightly above line  $y = 5$  ( $\text{HCO}_3^-/\text{SiO}_2$  ratio) in area 3, depicting an ambiguous character and reinforcing that they have an ionic composition between Groups 1 and 2.

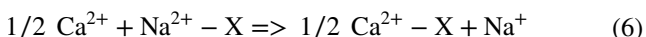
Other studies report significant releases of ions such as  $\text{Na}^+$ ,  $\text{Ca}^{2+}$ ,  $\text{Mg}^{2+}$ ,  $\text{HCO}_3^-$  into the groundwaters due to the natural process influencing water chemistry in the groundwater–rock interaction from carbonate and silicate weathering/dissolution (e.g., Madhav et al. 2021; Okofo et al. 2021).

**The chloro-alkaline index-CAI (Schoeller 1965)**

This index is calculated to assess the potential for ion-exchange reactions between groundwater and mineral constituents in aquifers. CAI also indicates whether an aquifer is salinizing

or freshening or has gone through these processes in the past. (Tiwari et al 2019; Stuyfzand 2008).

The ion exchange can be of the type called "base ion exchange process", in which  $Mg^{2+}$  and/or  $Ca^{2+}$  ions in the water are exchanged for  $Na^+$  and/or  $K^+$  from the mineral aquifer matrix. This is a softening process, since  $Ca^{2+}$  and  $Mg^{2+}$  are removed from the aqueous phase, reducing the water hardness. On the other hand, in the mechanism called "reverse ion exchange process", the opposite occurs (or hardening), that is, sequestration of  $Na^+$  and  $K^+$  ions by the mineral matrix of the aquifer and releasing of  $Ca^{2+}$  and/or  $Mg^{2+}$  ions to the aqueous phase. Reaction 6 presents an example of an ion-exchange reaction involving  $Ca^{2+}$  and  $Na^+$  (Hounslow 1995; Appelo and Postma 2005)



→Base cation exchange, softening, or freshening process→←Reverse cation exchange, hardening, or salinizing process←where X = solid exchanger (mainly clay and hydroxides minerals)

The CAI was calculated using the Schoeller (1965) formula

$$CAI = [Cl^- - (Na^+ + K^+)]/Cl^-(meq/L). \quad (7)$$

CAI values will be positive if there is a hardening process, negative if a softening process is present, and there is no ion-exchange process if CAI values are close to zero (Abu-alnaee et al. 2018; Tiwari et al. 2019). The scatter plot CAI values versus  $Cl^-$  concentrations (Fig. 8a) show that ANG-22 (Group 4) has CAI slightly higher than zero, indicating no ion exchange or a hardening (salinization) process, confirming the effect of seawater intrusion and saltwater upcoming

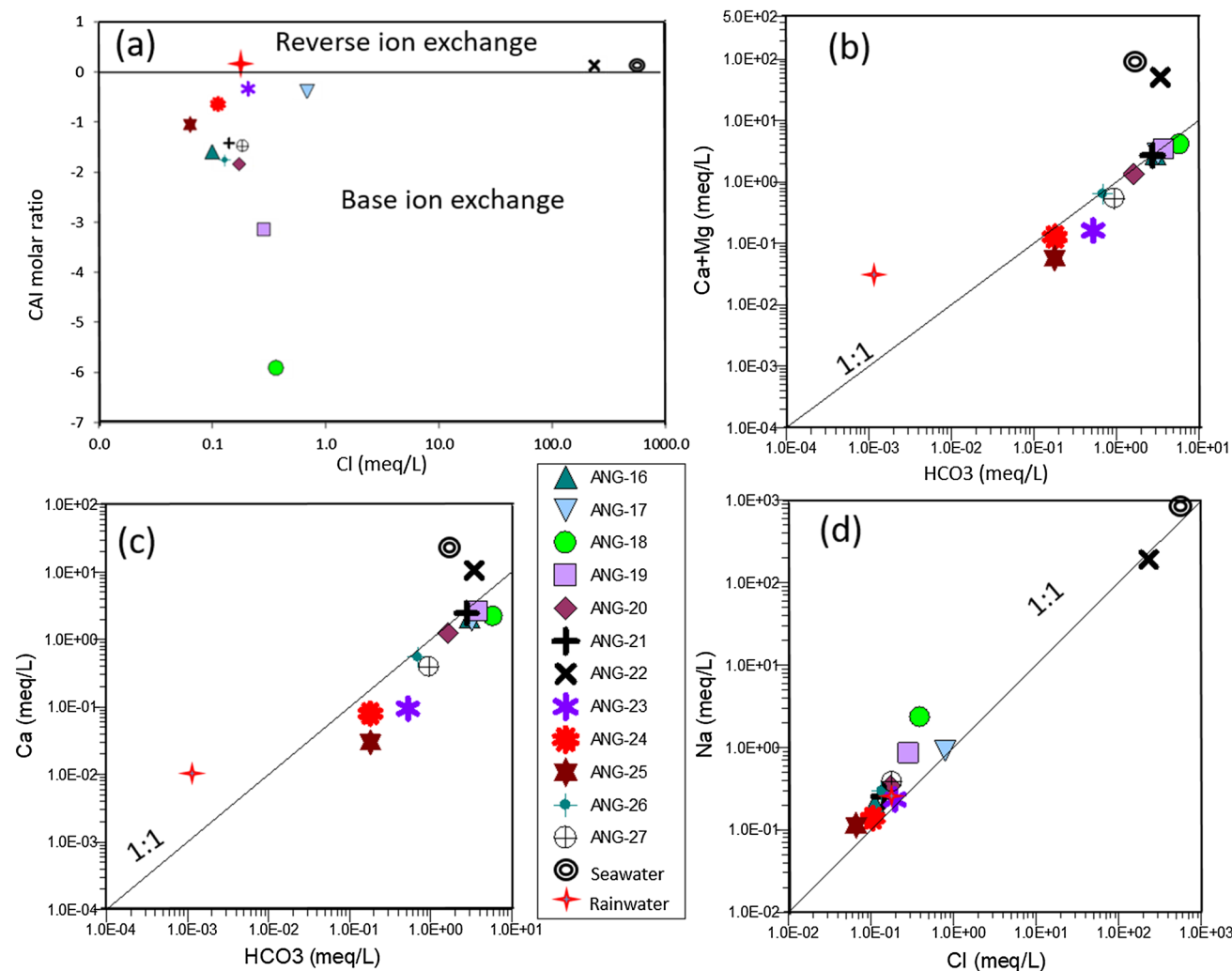


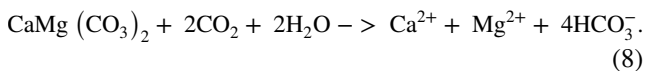
**Fig. 8** Scatter plot of **a** CAI versus  $Cl^-$  (meq/L), **b**  $Ca^{2+} + Mg^{2+}$  versus  $HCO_3^-$ , **c**  $Ca^{2+}$  versus  $HCO_3^-$ , and **d**  $Na^+$  versus  $Cl^-$ . The values of seawater and rainwater, respectively, from Millero (2013) and Souza et al. (2006)

for this water sample. The other samples (Groups 1 to 3) presented  $CAI < 0$ , indicating the potential for softening or freshening process, where  $Ca^{2+}$  decreases and  $Na^+$  increases in the aqueous phase.

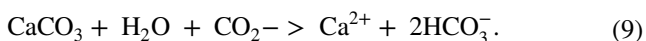
This indication of a possible ion-exchange softening process in the shallow porous aquifer at Itaorna Beach, the NPP site, should be pointed out. In radium-contaminated water, an artificial cation exchange resin can be used for removing  $Ra^{2+}$  (EPA 1983; Nirdosh 1984; Bi et al. 2016; Robin et al. 2017). Thus, theoretically, in case of an accidental release of radionuclides from NPP to the aqueous phase, the fluvial–marine clays can capture  $Ra^{2+}$ , releasing  $Na^+$  for instance, and mitigating groundwater radium contamination.

### Scatter plots ( $Ca^{2+} + Mg^{2+}$ ) versus $HCO_3^-$ (Fig. 8b) and $Ca^{2+}$ versus $HCO_3^-$ (Fig. 8c)

These plots were done to identify the potential sources of  $Ca^{2+}$  and  $Mg^{2+}$  (Shamsi et al. 2019). Figure 8b shows that the sample ANG-22 (Group 4) has an excess of ( $Ca^{2+} + Mg^{2+}$ ), as indicative of seawater, enriched mainly in  $Mg^{2+}$  (Millero 2013) and the reverse ion-exchange process (hardening). Regarding the other samples, it is observed that most of them (Group 2) fall on the 1:1 stoichiometric equilibrium line ( $Ca^{2+} + Mg^{2+}$ ) versus  $HCO_3^-$ , suggesting dissolution of dolomite or Mg-rich calcite according to reaction 8 (Hounslow 1995; Appelo and Postma 2005). However, some (Groups 1 and 3 samples) fell slightly below line 1:1, suggesting a base ion-exchange process (softening)



In Fig. 8c, except for the ANG-22 sample (Group 4), all samples fall close to or below the 1:1 stoichiometric equilibrium line  $Ca^{2+}$  versus  $HCO_3^-$ . The samples on the line suggest waters' composition with the main contribution of calcite weathering, according to reaction 9 (Hounslow 1995; Appelo and Postma 2005). The samples below the 1:1 line suggest a  $Ca^{2+}$  deficit, which may be due to calcium capture by the aquifer's solid phase (mainly clays) in an ion-exchange process (softening) involving  $Na^+$  (mostly Group 1). The indications provided by these plots (Fig. 8b and c) are consistent with the previous observations



### Scatter plot $Na^+$ versus $Cl^-$

This plot is used to identify potential sources of  $Na^+$  and  $Cl^-$  (Shamsi et al. 2019). Figure 8d clearly shows that, for the ANG-22 sample (Group 4), the source of  $Na^+$  and  $Cl^-$  is the seawater, which confirms the strong influence of

seawater on the ionic composition of this sample. Most of the data are slightly above the halite dissolution line. The  $Na^+/Cl^-$  ratio greater than 1 indicates either the presence of silicate weathering or base ion exchange (softening) between  $Na^+$  and  $Ca^{2+}$  (Shamsi et al. 2019). For Group 2 samples, it is suggested that ion exchange (Ca–Na) is the leading cause for  $Na^+$  excess. For samples from Groups 1 and 3, both processes must occur, whereas for samples ANG-23 to ANG-25 (Group 1), it is suggested that the excess of  $Na^+$  is predominantly due to the weathering of sodium-rich silicates (Na-rich plagioclase). These observations confirm the interpretation performed in Fig. 8a, b, and c. In other words, these data show a  $Na^+$  enrichment and concomitant  $Ca^{2+}$  depletion in most of the water samples, except for the ANG-22 sample, in which the saline influence is significant.

In summary, the chloro-alkaline index suggests the occurrence of base ion exchange in the waters of Groups 1 to 3, with the aqueous phase enriching in sodium and depleting in calcium. The waters of Group 1 occur in a hillside environment, where it predominates granitic–gneissic basement outcrops, residual soil, talus deposits, and dense vegetation, characterizing an aquifer recharge zone, but with occurrences of discharge points from the fractured aquifer. Where the fluvial–marine sediments prevail, the waters of Groups 2 and 3 are present, in addition to Group 4, which is the closest point to the sea. The waters in Group 1 are Ca– $Na^+$ – $HCO_3^-$ , not very mineralized (TDS < 70 mg/L), with ionic composition indicative of the weathering of granite–gneissic rocks. Based on the Gibbs diagram, Group 1 is in the rainfall dominance zone, which indicates that the rainwater infiltration is the main factor governing its chemical composition. Group 2 consists of  $Ca^{2+}$ – $HCO_3^-$  waters, more mineralized (100–500 mg/L TDS) than those of group 1, with ionic composition indicative of carbonate weathering, with rock dominance (Gibbs diagram), which indicates that the dissolution of rock-forming mineral is the main factor controlling the water chemistry of this group. Group 3 has intermediate hydrochemical characteristics between groups 1 and 2. For example, it has 70–100 mg/L TDS. The sample that characterized Group 4 clearly shows some interference from seawater, such as 20,000 mg/L of TDS and indicative of halite dissolution. In the Gibbs diagram, the sample fell in the typical evaporation dominance zone, indicating that the evaporation of seawater is the predominant factor in its chemical composition.

### Conclusions

The study area is characterized by a porous, free and shallow aquifer, consisting of talus deposits, residual soil, and marine to marine–fluvial sediments, occurring predominantly in the coastal plain. A fractured aquifer,

with a granite–gneissic composition, generally occurring under the porous aquifer but outcropping in the hills and hillsides. Based on the hydrochemical assessment, four types of water were identified in the shallow aquifer. From the hillsides towards the coastline, the research results suggest a hydrochemical evolution of local groundwater from Group 1 (high rainwater influence), passing through Group 3 (intermediate between Group 1 and 2) and Group 2 (rock influence), to Group 4 (seawater like). The waters of groups 1 to 3 showed potential for base cation exchange (softening or freshening process), while in Group 4, the potential is for reverse cation exchange (hardening or salinizing process).

In a general hydrogeology context, the methods and techniques applied proved to be particularly efficient in identifying water sources, water mixtures, and the salinization and freshening processes involved. The results obtained so contribute to research scarcity in the study area (considering its relevance) and serve as a guide for decision-makers for improved water resources management. In addition to the local diagnosis and hydrological dynamic assessment, which has large importance for the local economy and population health, the study is about a hydrogeologic scenario that can be easily found in other parts of the world. The freshening cation exchange identified in the shallow aquifer in Itaorna Beach is noteworthy. In case of an accidental release of radionuclides from the Nuclear Power Plants to the aqueous phase, the local clay lenses can capture  $Ra^{2+}$  in a natural contamination attenuation process.

Considering the anthropic activity and the natural hydrogeological context, more attention should be given to the groundwater dynamics in the area. The results from groundwater chemistry and processes obtained in this work can be used to obtain information on the general flow pattern and its interactions (e.g., with seawater) and as a first step towards building a conceptual framework of the area using groundwater models, to allow a better diagnosis and/or prognosis of groundwater use scenarios and/or contamination prevention.

**Acknowledgements** The authors would like to thank the International Atomic Energy Agency (IAEA) for funding this research through Coordinated Research Project—CRP F3302 and to Mr. Umayya D. S. Kumar the Project Officer (PO). We also wish to thank Eletronuclear for its technical and operational support.

**Funding** International Atomic Energy Agency (IAEA).

**Data availability** Not applicable.

**Code availability** Not applicable.

## Declarations

**Conflict of interest** The author declare that they have no conflict of interest.

**Ethical approval** Not applicable.

**Consent to participate** Not applicable.

## References

- Abu-alnaeem MF, Yusoff I, Ng TF, Alias Y, Raksmei M (2018) Assessment of groundwater salinity and quality in Gaza coastal aquifer, Gaza Strip, Palestine: an integrated statistical, geostatistical and hydrogeochemical approaches study. *Sci Total Environ* 615:972989
- APHA American Public Health Association (1999) Standard methods for the examination of water and wastewater. American Public Health Association, Washington
- Appelo CAJ, Postma D (2005) *Geochemistry, groundwater and pollution*, 2nd edn. Balkema, Rotterdam, p 634
- Bi Y, Zhang H, Ellis BR, Hayes KF (2016) Removal of radium from synthetic shale gas brines. *Environ Eng Sci* 33(10):2016. <https://doi.org/10.1089/ees.2016.0002>
- Bocanegra E, Da Silva Jr GC, Custodio E, Manzano M, Montenegro S (2010) State of knowledge of coastal aquifer management in South America. *Hydrogeol J* 18:261–267
- Bodrud-Doza Md, Bhuiyan MAH, Islam SMD-U, Rahman MS, Haque MdM, Fatema JK, Ahmed N, Rakib MA, Rahman MdA (2019) Hydrogeochemical investigation of groundwater in Dhaka City of Bangladesh using GIS and multivariate statistical techniques. *Groundw Sustain Dev* 8:226–244. <https://doi.org/10.1016/j.gsd.2018.11.008>
- Brimblecombe P (1986) *Air composition and chemistry*, VIII. Cambridge University Press, p 224
- Chadha DK (1999) A proposed new diagram for geochemical classification of natural waters and interpretation of chemical data. *Hydrogeol J* 7:431–439
- CPRM – Serviço Geológico do Brasil (2007) *Geologia da Folha Angra dos Reis SF.23-Z-CII (escala 1:100.000)*: Ministério das Minas e Energia, Brasília (2007). Available in: <https://rigeo.cprm.gov.br/handle/doc/10310>
- Eletronuclear (2005) *Estudo de Impacto Ambiental Unidade 3 da Central Nuclear Almirante Álvaro Alberto – ANGRA 3 – volume 2, maio de 2005*
- EPA US Environmental Protection Agency Group (1983) *Radionuclide Removal for Small Public Water System*. Technical Report. Washington, DC, p 162
- Gibbs RJ (1970) Mechanisms controlling world water chemistry. *Science* 170:1088–1090. <https://doi.org/10.1126/science.170.3962.1088>
- Guedes E, Heilbron M, Vasconcelos PM, Valeriano CM, Almeida JCH, Teixeira W, Thomaz Filho A (2005) K-Ar and 40Ar/39Ar ages of dikes emplaced in the onshore basement of Santos Basin, Resende area, SE Brazil: implications for the South Atlantic opening and Tertiary reactivation. *J S Am Earth Sci* 18:371–382
- Hounslow AW (1995) *Water quality data: analysis and interpretation*. CRC Press LLC, Lewis Publishers, Boca Raton
- IAEA International Atomic Energy Agency (2021) *Use of Isotope Hydrology to Characterize Groundwater Systems in the Vicinity of Nuclear Power Plants*. MONOGRAPH, Results of a Coordinated Research Project (CRP) F33022, 2016–2020. Vienna, p 199
- Khan F, Krishnaraj S, Raja P, Selvaraj G, Cheelil R (2021) Impact of hydrogeochemical processes and its evolution in controlling groundwater chemistry along the east coast of Tamil Nadu and Puducherry, India. *Environ Sci Pollut Res* 28:18567–18588. <https://doi.org/10.1007/s11356-020-10912-y>

- Madhav S, Raju NJ, Ahamad A, Singh AK, Ram P, Gossel W (2021) Hydrogeochemical assessment of groundwater quality and associated potential human health risk in Bhadohi environs, India. *Environ Earth Sci* 80(585):1–14. <https://doi.org/10.1007/s12665-021-09824-y>
- Martin L, Suguio K, Flexor J, Dominguez JML, Bittencourt ACSP (1996) Quaternary sea-level history and variation in dynamics along the Central Brazilian Coast: consequences on coastal plain construction. *An Acad Bras Ciências* 68(3):303–354
- Mechal A, Shube H, Godebo TR, Walraevens K, Birk S (2022) Application of multi-hydrochemical indices for spatial groundwater quality assessment: Ziway Lake Basin of the Ethiopian Rift Valley. *Environ Earth Sci* 81(25):1–22. <https://doi.org/10.1007/s12665-021-10135-5>
- Millero FJ (2013) Chemical oceanography, 4th edn. CRC Press, p 591
- Nandakumaran P, Balakrishnan K (2020) Groundwater quality variations in Precambrian hard rock aquifers: a case study from Kerala, India. *Appl Water Sci* 10:2. <https://doi.org/10.1007/s13201-019-1084-8>
- Nirdosh I (1984) Radium in uranium mill tailings—some observations on retention and removal. *Hydrometallurgy* 12:151–176
- Okoko LB, Anderson NA, Bedu-Addo K, Armoo EA (2021) Hydrochemical peculiarities and groundwater quality assessment of the Birimian and Tarkwaian aquifer systems in Bosome Freho district and Bekwai municipality of the Ashanti Region, Ghana. *Environ Earth Sci* 80(818):1–22. <https://doi.org/10.1007/s12665-021-10081-2>
- Papazotos P, Koumantakis I, Vasileiou E (2019) Hydrogeochemical assessment and suitability of groundwater in a typical Mediterranean coastal area: a case study of the Marathon basin, NE Attica, Greece. *HydroResearch* 2:49–59. <https://doi.org/10.1016/j.hydres.2019.11.002>
- Piper AM (1944) A graphic procedure in the geochemical interpretation of water analyses. *Trans Am Geophys Union* 25:914–923
- Rajaveni SP, Nair IS, Bhola PK, Zabel A, Monnikhoff B, Elango L (2021) Identification of management options to mitigate seawater intrusion in an overexploited multi-layered coastal aquifer by integrated rainfall–runoff, surface water and density-dependent groundwater flow modeling. *Environ Earth Sci* 80(617):1–24. <https://doi.org/10.1007/s12665-021-09836-8>
- Robin V, Tertre E, Beaucaire C, Regnault O, Descostes M (2017) Experimental data and assessment of predictive modeling for radium ion-exchange on beidellite, a swelling clay mineral with a tetrahedral charge. *Appl Geochem* 85:1–9. <https://doi.org/10.1016/j.apgeochem.2017.07.009>
- Sarkar M, Pal SC, Islam ARMdT (2022) Groundwater quality assessment for safe drinking water and irrigation purposes in Malda district, Eastern India. *Environ Earth Sci* 81(52):1–20. <https://doi.org/10.1007/s12665-022-10188-0>
- Schoeller H (1965) Qualitative evaluation of groundwater resources. *Methods Tech. Groundw. Investig. Dev. UNESCO*, pp. 54e83
- Sefie A, Aris AZ, Ramli MF, Narany TS, Shamsuddin MKN, Saadudin SB, Zali MA (2018) Hydrogeochemistry and groundwater quality assessment of the multilayered aquifer in Lower Kelantan Basin, Kelantan, Malaysia. *Environ Earth Sci* 77:397. <https://doi.org/10.1007/s12665-018-7561-9>
- Shamsi A, Karami GH, Hunkeler D, Taheri A (2019) Isotopic and hydrogeochemical evaluation of springs discharging from high-elevation karst aquifers in Lar National Park, northern Iran. *Hydrogeol J* 27(2):655–667. <https://doi.org/10.1007/s10040-018-1873-4>
- Silva-Filho EV, Sobral Barcellos RG, Emblanch C, Blavoux B, Sella SM, Daniel M, Simler R, Wasserman JC (2009) Groundwater chemical characterization of a Rio de Janeiro coastal aquifer, SE e Brazil. *J South Am Earth Sci* 27:100108
- Souza PA, Mello WZ, Maldonado J (2006) Composição química da chuva e aporte atmosférico na Ilha Grande. *RJ Quim Nova* 29(3):471–476
- Stuyfzand PJ (2008) Base exchange indices as indicators of salinization or freshening of (coastal) aquifers. 20th Salt Water Intrusion Meeting. Naples, Florida, USA
- Tiwari S, Chate DM, Bisht DS, Srivastava MK, Padmanabhamurty B (2012) Rainwater chemistry in the North Western Himalayan Region, India. *Atmos Res* 104–105(2012):128–138
- Tiwari AK, Pisciotta A, De Maio M (2019) Evaluation of groundwater salinization and pollution level on Favignana Island, Italy. *Environ Pollut* 249(2019):969–998. <https://doi.org/10.1016/j.envpol.2019.03.016>
- Tizro AT, Voudouris KS (2008) Groundwater quality in the semi-arid region of the Chahardouly basin, West Iran. *Hydrol Process* 22(6):3066–3078
- UFRJ Universidade Federal do Rio de Janeiro – Instituto de Geociências (2003) Levantamento e Diagnóstico Ambiental (Meio Físico) da Área de Influência da Central Nuclear (CNAEA) – Volume II, Eixo 2 – Geologia e Recursos Hídricos. UFRJ, Rio de Janeiro
- Xiao Y, Liu K, Yan H, Zhou B, Huang X, Hao Q, Zhang Y, Zhang Y, Liao X, Yin S (2021) Hydrogeochemical constraints on groundwater resource sustainable development in the arid Golmud alluvial fan plain on Tibetan plateau. *Environ Earth Sci* 80(750):1–17. <https://doi.org/10.1007/s12665-021-10076-z>
- Zeng Y, Zhou J, Zhou Y, Sun Y, Zhang J (2021) Causes of groundwater salinization in the plain area of Kashgar River Basin in Xinjiang, China. *Environ Earth Sci* 80(201):1–18. <https://doi.org/10.1007/s12665-021-10086-x>
- Zhang B, Zhang J (2021) The hydrological connection between fresh submarine groundwater discharge and coastal groundwater: an isotopic and a decadal hydrochemistry approach in an alluvial fan, central Japan. *Environ Earth Sci* 80(618):1–6. <https://doi.org/10.1007/s12665-021-09917-8>

**Publisher's Note** Springer Nature remains neutral with regard to jurisdictional claims in published maps and institutional affiliations.

Springer Nature or its licensor holds exclusive rights to this article under a publishing agreement with the author(s) or other rightsholder(s); author self-archiving of the accepted manuscript version of this article is solely governed by the terms of such publishing agreement and applicable law.